

An application of reliability-based robustness assessment of steel moment resisting frame structures under post-mainshock cascading events

Filipe L. A. Ribeiro ¹

André R. Barbosa ²

and Luís C. Neves ³

Abstract

The paper presented herein proposes a reliability-based framework for quantifying the structural robustness considering the occurrence of a major earthquake (mainshock) and subsequent cascading hazard events, such as aftershocks that are triggered by the mainshock. These events can significantly increase the probability of failure of buildings, especially for structures that are damaged during the mainshock.

The application of the proposed framework is exemplified through three numerical case studies. The case studies correspond to three SAC steel moment frame buildings of 3-, 9-, and 20- stories, which were designed to pre-Northridge codes and standards. Two-dimensional nonlinear finite element models of the buildings are developed using the Open System for Earthquake Engineering Simulation framework (OpenSees), using a finite-length plastic hinge beam model and a bilinear constitutive law with deterioration, and are subjected to multiple mainshock-aftershock seismic sequences.

For the three buildings analyzed herein, it is shown that the structural reliability under a single seismic event can be significantly different from that under a sequence of seismic events. The

¹Ph.D. Student, UNIC, Department of Civil Engineering, Faculdade de Ciências e Tecnologia - Universidade Nova de Lisboa, Quinta da Torre, 2829-516 Caparica, Portugal, and Visiting Ph.D. Student, School of Civil and Construction Engineering, Oregon State University, Corvallis, USA, E-mail: f.ribeiro@fct.unl.pt

²Assistant Professor, School of Civil and Construction Engineering, Oregon State University, 220 Owen Hall, Corvallis, OR 97331-3212, USA, E-mail: andre.barbosa@oregonstate.edu

³Lecturer, Nottingham Transportation Engineering Centre, Faculty of Engineering, University of Nottingham, Nottingham NG7 2RD, England, UK; Assistant Professor, UNIC, Department of Civil Engineering, Faculdade de Ciências e Tecnologia - Universidade Nova de Lisboa, Quinta da Torre, 2829-516 Caparica, Portugal, E-mail: luis.neves@nottingham.ac.uk

19 reliability-based robustness indicator used shows that the structural robustness is influenced by the
20 extent by which a structure can distribute damage.

21 **Keywords:** Aftershock, Nonlinear Dynamic Analysis, Robustness, Seismic Sequences.

22 INTRODUCTION

23 Structures in earthquake prone regions are susceptible to being damaged due to intense ground
24 motion shaking. Traditionally, design and analysis of building structures only considers one single
25 earthquake event, also known as a mainshock. However, in reality, structures can be subjected
26 to cascading events, defined as events likely to be triggered by a major earthquake, such as after-
27 shocks, fires, explosions, or tsunamis. The focus of this work is placed on sequences of ground
28 motions that include the mainshock as well as aftershocks. Structural damage is typically observed
29 in the large intensity mainshocks. Since the typical time interval between mainshocks and after-
30 shocks is small, structural repair or retrofit is not possible and the mainshock-damaged structures
31 are thus more susceptible to failure when an aftershock occurs. The term failure, as used herein, is
32 synonymous with exceeding a defined limit state that may render structures unfit for use (Newmark
33 and Rosenbleuth 1971).

34 In this paper, a measure of structural robustness is used to characterize the effect of aftershocks
35 on the seismic safety of structures. With respect to aftershocks triggered by mainshocks, a struc-
36 ture is said to be more or less robust depending on its capacity to sustain post-mainshock damage
37 without reaching failure. Three main approaches for quantifying structural robustness have been
38 proposed in the literature. In the first approach, measures of structural robustness are derived
39 from probabilistic risk assessments (Baker et al. 2008). Baker et al. (2008) defined a measure
40 for quantifying structural robustness as a function of direct and indirect risk. Even though this
41 approach is very powerful, the complexity and subjectiveness in the quantification of the direct
42 and indirect risk in large structural systems hinders the application of this approach. In the second
43 approach, measures of structural robustness are quantified in terms of ratios of structural properties
44 (e.g. damage, energy, or stiffness) between undamaged and damaged structures (Starossek 2006;
45 Cavaco et al. 2013). While these measures are useful in engineering practice, they fail to explicitly

46 describe failures. Finally, in the last approach, measures of structural robustness are defined as
47 a function of the probabilities of failure of the intact and damaged structure. Examples of such
48 measures are the indices presented by Frangopol and Curley (1987) and Lind (1995). It is worth
49 noting that, as discussed in Starossek and Haberland (2008), both these measures evaluate struc-
50 tural redundancy rather than robustness. However, for buildings, redundancy is provided by the
51 existence of alternative load paths which is the main mechanism providing robustness, rendering
52 these indicators an adequate indirect measure of structural robustness. Robustness assessment of
53 structures for cascading hazards is currently lacking in the literature.

54 There are two main challenges in modeling the effects of aftershock events on structures for
55 computing structural robustness. The first challenge is related to the accurate modeling of ex-
56 pected mainshock-aftershock seismic sequences. This has been discussed extensively in (Ruiz-
57 García 2012; Fragiacomano et al. 2004; Lee and Foutch 2004; Li and Ellingwood 2007; Luco et al.
58 2004; Luco et al. 2011; Ryu et al. 2011). Luco et al. (2011) and Ryu et al. (2011) performed
59 mainshock-aftershock incremental dynamic analyses (IDA, Vamvatsikos and Cornell 2002) on
60 single-degree-of-freedom models subjected to artificial sequences of mainshock-aftershock "back-
61 to-back" structural analyses. The second challenge is related to accurate modeling of the effects
62 of damage introduced by the mainshock on structural performance. To this effect, state-of-the-art
63 modeling for estimation of structural performance/damage can be found in ATC-72 (PEER/ATC
64 2010). In the ATC-72 report emphasis is placed on phenomenological models that capture the
65 main effects of strength and stiffness deterioration.

66 In this study, a probabilistic framework for the assessment of structural robustness under main-
67 shock triggered aftershocks is developed. Emphasis is placed on the evaluation of the structural ro-
68 bustness as a function of the probability of failure (or the reliability index) under different damage
69 scenarios. In the probabilistic methodology, nonlinear dynamic time-history analyses of structural
70 computational models of buildings are used to estimate the recorded structural damage due to mul-
71 tiple mainshock-aftershock sequences. Mainshock and aftershock incremental dynamic analyses
72 are carried out following the approach proposed by Ryu et al. (2011), where artificial mainshock-

73 aftershock sequences are used in the "back-to-back" nonlinear dynamic time-history analyses. This
74 approach is applied to multi-degree-of-freedom (MDOF) structural models of the 3-, 9-, and 20-
75 story steel moment resisting frames (SMRFs) of the SAC steel project (FEMA355C 2000). The
76 analytical building models are developed using the Open System for Earthquake Engineering Sim-
77 ulation, OpenSees (Mazzoni et al. 2009), and were validated using the numerical data available
78 in the literature (FEMA355C 2000; Luco 2002). Important aspects of beam strength and stiffness
79 degradation as damage progresses during the analysis were also included in the model. To quan-
80 tify the damage due the mainshock and aftershock, the buildings are first subjected to a mainshock
81 incremental dynamic analysis and for each level of the intensity of the mainshock, the mainshock-
82 damaged structure is then subjected to incremental dynamic analysis due to the aftershocks.

83 **FRAMEWORK**

84 The framework proposed for the assessment of the structural robustness of buildings is sche-
85 matically presented in Figure 1. The first step of the analysis corresponds to the definition of
86 the engineering measures considered to define failure and the thresholds used to define the per-
87 formance or limit states. The following step of the analysis corresponds to the definition of the
88 mainshock hazard. This depends on the location of the building and the foundation soil. Extensive
89 data exists on the seismic hazard of locations in Europe, North America, and Japan (e.g., Petersen
90 et al. 2008). From this, the mean annual rate of exceeding a ground motion intensity measure
91 can be defined and, consequently, a probabilistic distribution of the mainshock intensity measure
92 can be obtained. The ground motion intensity measure most used is the 5% damped linear elastic
93 spectral acceleration at a fundamental period of the structure T_1 , which is denoted as $S_a(T_1)$ (e.g.
94 Baker 2007). Herein, the notation S will be used to refer to a spectral acceleration at a fundamental
95 period of the structure.

96 Based on the definition of the hazard, a set of mainshock ground accelerograms can be defined
97 (Step 3.1), considering either real or artificial accelerograms (e.g. Bommer and Acevedo 2004).
98 Considering the uncertainty in the characteristics of the mainshock, several different accelero-
99 grams should be used and methods for estimating the structural response due to the mainshock

100 are discussed in Baker (2007), for example. When probabilistic simulation is employed, a set
101 of mainshocks following the distribution of the spectral acceleration are used. In Step 3.2, finite
102 element models are defined, leading at sufficient accuracy to characterize the nonlinear response
103 to collapse, providing reliable estimates of the residual displacements and loss in stiffness and
104 strength. Details on an example of models that can be employed to account for the strength and
105 stiffness deterioration are described in the following section. In Step 3.3, the damage caused by
106 the mainshock is evaluated for each of these samples. In the present paper, this is done using an
107 incremental dynamic analysis (Vamvatsikos and Cornell 2002), but other methods for estimating
108 the damage conditional on the mainshock ground motion intensity measure can be defined. Based
109 on the results of these analyses, in Step 3.4, the probability of failure under mainshock alone (p_{f1})
110 can be estimated using:

$$111 \quad p_{f1} = \int_{S^m} P(F|S^m = s^m) dP(S^m) \quad (1)$$

112 where S^m represent the ground motion spectral accelerations associated with the mainshock at
113 the fundamental period of the intact structure, $P(S^m)$ corresponds to the annual probability of
114 occurrence of a spectral acceleration associated with the mainshock, and $P(F|S^m = s^m)$ repre-
115 sents the probability of failure F conditional on S^m . The probabilities of exceedance of a given
116 S^m are defined considering, for example, the data described in Petersen et al. (2008). According
117 to Jayaram and Baker (2008) the spectral accelerations follow lognormal distributions. The term
118 F describes a failure event, which is defined as exceedance of a limit state. When considering a
119 collapse limit state, for example, FEMA356 (2000) reports 5% as a limiting value interstory drift
120 ratio in buildings. It is worth noting that Eq.1 is applicable for any limit state.

121 Based on the properties of the mainshock, the conditional aftershock hazard can be defined
122 in Step 4. The occurrence rate and the distribution of aftershocks have strong correlations with
123 mainshock magnitude (Yeo and Cornell 2005). As a consequence, an aftershock hazard should
124 be defined considering the mainshock amplitude, frequency content, and duration. Therefore, the
125 simulation of mainshock-aftershock ought to be performed with real sequences. However, for

126 most sites such information is not available, and a general formulation cannot rely on existence of
 127 this data. Thus, artificial mainshock-aftershock sequences are used herein, following Luco et al.
 128 (2011), Ryu et al. (2011), and Li et al. (2012). In Step 5.1 a set of aftershock ground accelerations
 129 is defined. In Step 5.2, damage resulting from mainshock and aftershock is evaluated, following
 130 the tasks described above for the mainshock alone. The probability of failure due the aftershock
 131 conditional on the occurrence of a mainshock that does not lead to failure, p_{f2} , can be computed
 132 through:

$$133 \quad p_{f2} = \frac{p_{f3} - p_{f1}}{1 - p_{f1}} \quad (2)$$

134 where the probability of failure considering both mainshock and aftershock, computed in Step 5.3,
 135 is given by:

$$136 \quad p_{f3} = \int_{S^m} \int_{S^a} P(F|S^m = s^m, S^a = s^a) dP(S^a|S^m = s^m) dP(S^m) \quad (3)$$

137 and where S^a represent the ground motion spectral accelerations associated with the aftershock
 138 at the fundamental period of the intact structure, $P(S^a|S^m = s^m)$ is the conditional probability
 139 of occurrence of an aftershock with spectral acceleration S^a following a mainshock with spectral
 140 acceleration S^m , and $P(F|S^m = s^m, S^a = s^a)$ represents the probability of failure F conditional
 141 on S^m and S^a . S^a is also assumed to follow a lognormal distribution.

142 In Step 6, the robustness assessment is performed based on the comparison of the reliability
 143 index ($\beta = -\Phi^{-1}(p_f)$) of the undamaged structure β_{intact} , which accounts for the mainshock only,
 144 with the reliability index of the mainshock-damaged structure $\beta_{damaged}$ as (Frangopol and Curley
 145 1987):

$$146 \quad \beta_R = \frac{\beta_{intact}}{\beta_{intact} - \beta_{damaged}} \quad (4)$$

147 where $\beta_{intact} = -\Phi^{-1}(p_{f1})$ and $\beta_{damaged} = -\Phi^{-1}(p_{f2})$.

148 Herein, the reliability index for the mainshock β_{intact} is computed considering the spectral ac-

149 celeration event space divided in 10 intervals for ten equally likely ground motion records each
150 denoted as earthquake E_j using a technique known as Stratified Sampling (Kiureghian 1996). The
151 reliability index for the aftershock $\beta_{damaged}$ is computed using stratified sampling for the main-
152 shock spectral acceleration and considering the conditional probability of failure due to aftershock
153 as the probability of exceedance of the minimum aftershock spectral acceleration leading to fail-
154 ure. The probability of failure is computed considering the combination of 10 mainshock and 10
155 aftershock ground motion records. In this computation it is assumed herein that the mainshock and
156 the aftershock ground motion spectral acceleration are uncorrelated.

157 **BUILDING MODELS**

158 **General Description**

159 The steel moment resisting frame (SMRF) buildings studied in this work are a subset of the
160 models developed as part of the SAC Steel project (FEMA355C 2000). The buildings included
161 in this study are a 3-, a 9-, and a 20-story buildings (denoted LA3, LA9 and LA20, respectively)
162 which were designed for Los Angeles using pre-Northridge codes (UBC 1994). In all buildings,
163 external frames were designed to resist the lateral seismic loads and interior frames were designed
164 as gravity frames. As shown in Figure 2, all buildings have spans of 9.15m in both directions.
165 The 3-story building presents no basement, while the 9- and 20-story buildings have one and two
166 basement levels, respectively. The height of the frames is constant and equal to 3.96m, except for
167 the first level of the two taller buildings, which have a height of 5.49m, as shown in Figure 2. A
168 detailed description of the buildings can be found in FEMA 355C (2000) and Luco (2002).

169 Two-dimensional centerline models of an external frame of each of the three buildings are used
170 for the structural analysis. According to one of the modeling alternatives presented in Luco and
171 Cornell (2000), strong-column weak-beam ductile behavior was assumed for all structures. Brittle
172 mechanisms and connection fracture modes were not considered.

173 Geometric nonlinearities are accounted for during the analysis by considering a $P - \Delta$ leaning
174 column. A rigid diaphragm is assumed for each floor. Soil-structure interaction was not considered.
175 Masses and loads are applied to beam-column joints. Similarly to what was defined in FEMA355C

176 (2000), Rayleigh damping is assigned to the models. As described in Erduran (2012), a damping
177 ratio of 2% was assigned to the first mode and a higher mode. Following FEMA355C (2000) the
178 higher mode considered is the fifth mode for LA20 and a mode with period 0.2s for buildings LA3
179 and LA9 (a period close to the LA3's 3rd modal period and the LA9's 5th modal period).

180 **Component Modeling**

181 The building's nonlinear behavior was modeled considering a set of four different models for
182 each structure, as described in Table 1. The four models considered differ in the method used to
183 simulate the beams. For the first two models, a zero-length plastic hinge element is used, consid-
184 ering elasto-plastic behavior with hardening and a bilinear model with deterioration (*Bilin* model
185 in OpenSees). The third and fourth models used the same material models, but consider a finite-
186 length plastic hinge element. In all four cases, the columns were modeled considering a distributed
187 plasticity model and an elasto-plastic constitutive law with a 3% hardening rate assigned to each
188 fiber. A moment-curvature section analysis showed that this corresponds to a section hardening of
189 3.0%, consistent with the assumptions used in the FEMA355C modeling. Thus, for the columns,
190 the main phenomenon considered is the interaction between moment and axial load. This as-
191 sumption is supported by recent testing (Newell and Uang 2008), where it is shown that columns
192 such as the ones being modeled do not exhibit deterioration in strength by more than 10% for
193 $P/P_y \leq 0.75$ even at 8% story drift ratios. For the building under analysis, which was designed
194 using the strong-column-weak-beam assumption, only minor deterioration in stiffness and strength
195 of columns is expected, and disregarding these effects will have no significant impact on the re-
196 sults. However, for buildings consisting of slender columns, this assumption may not hold and the
197 effect of deterioration of the strength and stiffness of the columns should be evaluated.

198 *Zero-Length vs. Finite-Length Plastic Hinge Elements*

199 Model idealizations for nonlinear structural analysis of beams range from phenomenologi-
200 cal models, such as concentrated plasticity models and finite-element distributed plasticity beam-
201 column elements, to complex continuum models based on plane-stress or solid finite-elements. In
202 the concentrated plasticity models (Giberson 1969), nonlinear zero-length springs are discretized

203 at both ends of a linear-elastic beam-column element. These elements have been recently pro-
204 posed as the main method for estimating seismic demands (Ibarra and Krawinkler 2005; Medina
205 and Krawinkler 2005; Haselton and Deierlein 2007) and are the preferred modeling approach in the
206 Applied Technology Council ATC-72 modeling guidelines proposed recently (PEER/ATC 2010).
207 Considering that zero-length models have been widely used to model the seismic performance of
208 buildings, in this work they are used as a reference, and the results obtained using the finite length
209 plastic hinge elements are compared with those to ascertain their accuracy.

210 Scott and Fenves (2006) proposed a novel approach for modeling nonlinear behavior of frame
211 structures based on a force-based finite-length plastic hinge beam-column elements (*beam with*
212 *hinges*) which overcomes issues related to localization phenomena observed in distributed plastic-
213 ity beam-column elements (Coleman and Spacone 2001). Furthermore, finite-length plastic hinge
214 elements can model plastic hinge length explicitly and separate the behavior of beam in the span
215 from that of beam-column connections. Compared to zero-length springs, finite-length plastic
216 hinge elements allow faster model development due to the reduction in the number of nodes and
217 elements.

218 *Elasto-plastic Model with Kinematic Hardening vs. Bilinear Model With Deterioration*

219 Steel structures are traditionally modeled considering an elasto-plastic behavior with kinematic
220 hardening, accounting for Bauschinger effect. However, during an earthquake, structural elements
221 are subjected to large inelastic cyclic deformations which lead to deterioration of both strength
222 and stiffness properties of components, affecting the overall structural performance under seismic
223 loading.

224 In the present work, a modified version of the Ibarra-Krawinkler (2005) phenomenological
225 model, applicable to any force-deformation relationship, is employed to simulate beam behavior
226 and compared to an bilinear model with kinematic hardening. This model was used by Lignos and
227 Krawinkler (2011) to model the moment-rotation relationship of plastic hinges in steel elements.
228 The model considers strength and stiffness deterioration, defined in terms of element geometry,
229 material properties, and cross-section geometry.

230 The model by Lignos and Krawinkler (2011) defines a moment-rotation relationship and, con-
231 sequently, can not be directly applied when a finite length plastic hinge is considered, which re-
232 quires the use of a moment-curvature relationship. Based on the moment-rotation model described
233 above, it is possible to define the moment-curvature $M - \chi$ model by scaling the moment-rotation
234 backbone curve, as well as, the loading and unloading rules, in terms of the length of the plas-
235 tic hinge, L_p , resulting in the model presented in Figure 3. This plastic hinge moment-rotation
236 model is based on the assumption of a double curvature deformation, which leads to an elastic
237 stiffness of $6EI/L$. When a finite length plastic hinge element is used, a plastic hinge length of
238 $L_p = L/6$ should be used to recover the exact solution for the case of a fixed-fixed beam column
239 element (Scott and Ryan 2013). All other model parameters are defined as proposed in (Lignos
240 and Krawinkler 2011; Lignos and Krawinkler 2012). Axial and shear behavior is assumed to be
241 linear elastic. Joint shear deformations (e.g. Gupta and Krawinkler 1999) and fracture due to low
242 cycle fatigue (Lignos et al. 2011) are not included in this work.

243 For the building examples analyzed, the axial load expected to develop in beams is very low and
244 the interaction between axial load and bending moment in beams is significantly less relevant than
245 the deterioration of stiffness and strength which is expected to occur in the beams. For this reason,
246 the interaction between axial load and bending moment is disregarded for the beams. The modeling
247 assumptions made in this work are intended to provide a relatively simple structural model and,
248 at the same time, accurately simulate the deterioration of the steel members to collapse. Thus,
249 the modeling of some building components was neglected in these models, such as beam-column
250 joints, column base plate connections, and partially restrained connections. The influence of these
251 components in the robustness of steel structures to cascading events is worth studying in future
252 works.

253 **Model validation**

254 The four models described were compared to those developed by Luco and Cornell (2000),
255 also designated as *Model M1* (FEMA355C 2000), for the same buildings. The models in Luco
256 and Cornell (2000) were developed using the software *DRAIN-2DX* (Prakash et al. 1993). The

257 models implemented herein were developed in OpenSees. The elements used in the *DRAIN-2DX*
258 models correspond to concentrated plastic hinge models and a linear P-M interaction surface was
259 assumed for compressive axial loads greater than $0.15P_y$. While the model in FEMA355C (2000)
260 considered this simplified bilinear P-M interaction surface, the P-M interaction surface considered
261 herein is obtained implicitly during the analysis since the columns are modeled using fiber-section
262 nonlinear beam-column elements. A representation of the P-M interaction curve (at the section
263 level) is presented in Figure 2(d).

264 The model validation performed herein includes the comparison of results for both a nonlinear
265 static pushover and nonlinear dynamic time-history analysis. Furthermore, the buildings periods
266 available in the literature also correlate well with the ones obtained in the FE models developed in
267 this work, as shown in Table 2.

268 *Nonlinear Static Analysis*

269 The nonlinear static analyses were carried out considering the four models described in Table 1
270 and compared to those presented in FEMA355C (2000) and Luco (2002). The lateral load pattern
271 applied is proportional to the first mode of vibration of each structure.

272 Figures 4, 5, and 6 show the pushover curves for each of the three buildings and the four
273 finite element models used. For reference, these figures also show the design base shear quantified
274 according to the allowable stress design method (ASD) of the 1994 Uniform Building Code (UBC
275 1994). It can be seen from these figures that the overall match of the pushover curve are quite
276 good for the models with hardening. In the elastic range the differences for all models to the
277 results presented in FEMA355C (2000) are small, increasing slightly with the increase in building
278 height. In spite of the differences for the 20-story building being discernible in the elastic range,
279 as shown in FEMA355C (2000), such variations are expectable as a consequence, for example, of
280 alternative joints models. For all buildings, the models considering an elasto-plastic with hardening
281 constitutive law (FMRH, FZLH, and FEMA355) presented a similar behavior, showing that the use
282 of beam with hinges models does not affect significantly the results obtained. For the two taller
283 buildings, a softening behavior is observable in all models, as a result of $P - \Delta$ effects. When the

284 bilinear model with deterioration is considered (FMRB and FZLB) the post peak force decreases
285 faster, as a result of the strength deterioration considered for the beams. As a consequence of the
286 strong-column weak-beam design, plastic hinges form firstly in the beams. The use of the bilinear
287 model with deterioration (FMRB and FZLB) leads to a faster decrease in the post peak base-shear
288 force, as a result of softening in the beams and corresponding change in column moment gradient,
289 once the plastic hinges form.

290 In summary, the results of the pushover analysis show that the models using an elastic-plastic
291 constitutive law lead to results similar to those described in FEMA355C (2000). Secondly, the use
292 of zero-length and beam with hinges does not affect the results significantly, allowing the use of
293 the finite-length plastic hinges model in subsequent analysis. Finally, the use of the bilinear model
294 with deterioration for the beams produced larger strength reduction.

295 *Nonlinear Dynamic Time-History Analysis*

296 To compare the results described in Luco and Cornell (2000) with those resulting from the mod-
297 els used in this work, the structural response is evaluated considering forty (twenty two-component
298 records) SAC Steel Project LA01-LA40 earthquake records. Forty nonlinear dynamic time-history
299 response analyses were performed for each model and each of the three buildings. Obtained results
300 were compared to those presented by Luco and Cornell (2000) in terms of maximum interstory drift
301 ratio. The mean relative errors obtained for each model and building are presented in Table 3. For
302 the models considering an elastic-plastic behavior (FZLH and FMRH) the results are relatively
303 close, with a maximum mean error of 7.4%. Correlation between the floor levels where these
304 interstory drift ratios are observed for the models developed by Luco and Cornell (2000) and the
305 ones shown in this paper was also quite good (Ribeiro et al. 2012).

306 The model validation performed is considered to be sufficient for the FZLH and FMRH models.
307 Even though no direct validation of the FZLB and FMRB models with experimental results is
308 possible, the definition of component degradation is consistent with experimental results and P-M
309 interaction is considered explicitly. Considering the advantages of the finite length model described
310 and to include realistic effects of beam properties deterioration in the analysis, the FMRB model

311 is used in the subsequent analyses.

312 **ANALYSIS DESCRIPTION**

313 To evaluate the increased probability of failure associated with the occurrence of an aftershock
314 following a major earthquake, a simulation procedure was employed that considered as random
315 variables the spectral accelerations of the mainshock and the aftershock corresponding to the initial
316 fundamental period of the structure. Although the occurrence rate and distribution of aftershocks
317 are correlated to mainshocks magnitude (Yeo and Cornell 2005), their amplitude, frequency con-
318 tent, and duration are very difficult to simulate. Thus, artificial mainshock-aftershock sequences
319 are used herein, following Luco et al. (2011), Ryu et al. (2011), and Li et al. (2012).

320 **Numerical and Computational Methods**

321 The mainshock and aftershock are modeled considering a set of 10 accelerograms, each scaled
322 independently, representing different shaking intensities. For performing the incremental dynamic
323 analysis (IDA), each of the 10 mainshocks considered is scaled 10 times, by multiplying the corre-
324 spondent time-history record by the objective spectral acceleration, $S^m(T_1)$, divided by the original
325 ground motion spectral acceleration, $S^{GM}(T_1)$, corresponding to a stratified sampling of the spec-
326 tral accelerations. Each of the mainshocks can be followed by one of the 10 aftershocks. For
327 each aftershock an IDA is also performed for at least 20 intensity levels. Thus, in this analysis
328 the aftershock ground motion is incrementally scaled (by multiplying the time-history record by
329 $S^a(T_1)/S^{GM}(T_1)$), similarly to the procedure of a regular IDA, performing a number of n back-
330 to-back analysis, where n depends on the aftershock ground motion, the building being analyzed,
331 and the damage state at the end of the mainshock. Each aftershock incremental dynamic analysis
332 (AIDA) is computed considering the polarity of the aftershock (positive and negative directions).
333 A 30s time interval of free-vibration was considered between the end of the mainshock and the
334 application of the aftershock ground motion records. This duration was deemed sufficient after a
335 preliminary study that showed that the maximum nodal velocity observed during the last second
336 of this 30s interval was, for all buildings, smaller than 0.6% of the peak velocity observed for the
337 mainshock leading to highest drifts short of collapse.

338 For each run, the Newton-Raphson method is used for solving the nonlinear system of equa-
339 tions at each time step. To analyze the structure up to interstory drift ratios of 10%, a convergence
340 study of the horizontal roof peak displacement and horizontal peak floor absolute acceleration as
341 a function of the integration time step was performed. Time-steps considered were 0.01s, 0.005s,
342 0.002s, 0.001s, 0.0005s, 0.0001s, and 0.00005s. It was observed that a time step of 0.002s was
343 sufficiently small to produce negligible errors (when compared to the 0.00005s) and no significant
344 changes in the response were observed when smaller time steps were used.

345 To reduce the total computational time required for obtaining all the results for these large num-
346 ber of runs, an embarrassingly parallel computing framework was implemented. The implemented
347 framework makes use of the OpenSees (v2.4.0, release 5172) sequential version and a batch-queue
348 system called HTCondor (v7.8.0) (Thain et al. 2005). HTCondor is a specialized batch system for
349 managing computational-intensive jobs. To make the most use of two student computer centers of
350 Civil Engineering Departments at both Oregon State University (OSU) and Universidade Nova de
351 Lisboa (UNL), two HTCondor pools were created, consisting of 464-cores at OSU and 96-cores
352 at UNL. Since the research team was geographically dispersed, to minimize time needed for sim-
353 ulation data transfer and post-processing of the numerical results, a OSU-UNL web shared folder
354 was created using a commercial application.

355 **Ground Motion Records**

356 The ground motion records used in this study were selected from the set of forty SAC Steel
357 Project LA01-LA40 earthquake records mentioned above, considering earthquakes with the high-
358 est peak ground acceleration. These records were obtained from real and simulated ground mo-
359 tions, scaled so that their mean response spectrum matches the 1997 NEHRP design spectrum,
360 as reported by Somerville et al. (1997). The time histories for Los Angeles are all derived from
361 recordings of shallow crustal earthquakes on soil category D. The ten SAC records selected for
362 this study are characterized by a moment magnitude M_W between 6.0 and 7.4, duration between
363 29.9s and 59.9s, and peak ground acceleration between 0.6g and 1.3g. The ten E1 to E10 ground
364 motion records used correspond to SAC earthquakes: LA11, LA18, LA19, LA21, LA26, LA28,

365 LA30, LA31, LA36 and LA37.

366 In order to quantify the probability of failure of the structures, the spectral accelerations at Los
367 Angeles are estimated from the hazard curves generated for the 2008 National Seismic Hazard
368 Mapping Project (NSHMP) (Petersen et al. 2008) for soil type D. These are approximated by a
369 log-normal distribution, under the mild assumption that the findings of Jayaram and Baker (2008)
370 also hold for the modified ground motion records.

371 **DETERMINISTIC NONLINEAR DYNAMIC TIME-HISTORY RESPONSE ANALYSIS**

372 This section presents results obtained for representative nonlinear dynamic time-history re-
373 sponse analyses, selected from those described above. The performance of the LA3 building is
374 assessed considering a mainshock ground motion spectral acceleration of $1.2g$ and $0.9g$ for the
375 aftershock spectral acceleration. Earthquake ground motions E1 and E4 are used as the mainshock
376 and aftershock, respectively.

377 Figure 7 shows the time-history response of the LA3 building in terms of floor acceleration,
378 roof drift ratio, and interstory drift ratio during four identified time-periods (TP1-TP4): (i) TP1 -
379 duration of the mainshock; (ii) TP2 - free vibration period of 30s after the mainshock; (iii) TP3 -
380 duration of the aftershock; and (iv) TP4 - free vibration period of 30s after the aftershock. This
381 figure also shows the floor accelerations and the interstory drift ratios at the instants when peak
382 interstory drift ratio is attained during the mainshock and the aftershock, respectively. The peak
383 interstory drift ratio during the mainshock is 4.1% at the 3rd story. In Figure 8 two moment-rotation
384 responses are shown at two different elements. It is important to note that during the aftershock the
385 deformations are much larger, especially for beams, whose response go beyond the peak strength,
386 i.e. a softening response is observable.

387 The deformed shape of the LA3 building at the peak deformation instant is shown in Figure 9.
388 This figure also shows the deformed shapes of the LA9 and LA20 buildings, in which, for repre-
389 sentative analyses, the size of the circles illustrate the relative scales of rotations recorded at the
390 end of each element. For the LA3 building, almost all beam ends had gone into the inelastic regime
391 during the mainshock. Although the damage on the structure at the end of the mainshock is consid-

392 erable, as it can be inferred through the number of plastic hinges formed during the mainshock, the
393 residual deformation is not significant (see Figure 7). At the instant when the peak interstory drift
394 ratio is recorded during the aftershock, columns on the first story have formed plastic hinges in
395 both ends, which indicates that an undesirable soft story mechanism is formed. Four plastic hinges
396 have also formed in second story columns and two in the third one. Effects of higher modes in the
397 instants where peak interstory drifts are recorded can be observed in the LA9 and LA20 building
398 response especially during the aftershock (see Figure 9).

399 **AFTERSHOCK INCREMENTAL DYNAMIC ANALYSIS**

400 For each mainshock-aftershock combination and each mainshock intensity, an aftershock in-
401 cremental dynamic analysis (AIDA), for increasing aftershock intensities, is performed in order
402 to compute the failure probability under this sequence of events. In Figure 10, AIDA curves are
403 shown for four mainshock ground motion spectral accelerations. For sake of brevity only results
404 from the LA3 building are shown herein. Earthquake E5 is considered as mainshock. Ten AIDA
405 curves are then computed for the ten possible aftershocks. For each mainshock intensity, the results
406 obtained show the variation of the peak interstory drift ratio, θ_{max} , as a function of the aftershock
407 ground motion spectral acceleration.

408 The value of 10% of interstory drift ratio is considered to be the threshold for failure (Baker
409 2007). Higher values of interstory drift ratio will lead to violation of the performance threshold and
410 thus be considered as failure. Previous probability-based studies (e.g., Baker 2007) have concluded
411 that 10% IDR is an adequate threshold to define collapse in a numerical framework. Although
412 FEMA356 (2000) defines 5% IDR for collapse prevention, to study the structural robustness (i.e.,
413 the capacity of the structure to sustain damage) this larger value allows for the assessment of
414 the nonlinear structural behavior under very large deformations, which contributes to the accurate
415 evaluation of the reliability-based structural robustness by allowing for more accurate computation
416 of the probability of failure.

417 Figure 10 shows the AIDA curves illustrating the decrease in capacity with the increase in
418 the mainshock intensity. For example, the aftershock E4 ground motion spectral acceleration that

419 leads the structure to failure is $1.7g$ when the mainshock ground motion spectral acceleration is
420 $1.2g$, whereas when the mainshock ground motion spectral acceleration is $2.4g$ the aftershock
421 spectral acceleration that leads to failure is $1.1g$.

422 **ROBUSTNESS ASSESSMENT RESULTS**

423 Figure 11 shows the lowest aftershock spectral acceleration that leads the LA3 building to
424 fail ($\theta_{max} = 10\%$) versus the mainshock spectral acceleration. The figure corresponds to results
425 obtained using earthquake E_5 for both the mainshock and the aftershock. It can be seen that for
426 lower intensities of the mainshock there is little impact of mainshock on the aftershock spectral
427 acceleration that leads to failure. Additionally, for increasing mainshock intensities, the aftershock
428 spectral accelerations that lead to failure are reduced, since the mainshock induced damage reduces
429 the capacity of the structure to sustain additional damage due to the aftershocks. Since the same
430 accelerograms are used for generating both mainshock and aftershock, application of a mainshock
431 only or an aftershock following a low intensity mainshock (i.e., causing no damage to the structure)
432 are equivalent. Consequently, the lowest mainshock spectral acceleration leading to failure is
433 identical to the (minimum) aftershock spectral acceleration which leads to failure for very low
434 mainshock intensities.

435 In Figure 12 the median aftershock ground motion spectral acceleration that leads the structures
436 to failure is represented as a function of the median mainshock ground motion spectral accelera-
437 tion. A similar trend to that described for Figure 11 is observable here, but now for the entire
438 set of AIDA analyses considered. Figure 12 also shows the median residual displacements after
439 application of the mainshock. The results show a significant correlation between the increase in
440 residual displacements and the reduction in the aftershock leading to failure, indicating that resid-
441 ual displacements could be used as a measure of damage.

442 In Table 4, the probabilities of failure and the corresponding reliability indices are presented
443 considering mainshock, aftershock and mainshock+aftershock. The redundancy indicator, β_r , in-
444 troduced by Frangopol and Curley (1987) is used to compare robustness of the three buildings.
445 The reliability indices obtained considering only the mainshock are very similar across structures,

446 showing that the design procedure applied is consistent. However, the probability of failure consid-
447 ering aftershock and mainshock-induced damage increases much more significantly for buildings
448 LA3 and LA20, than for LA9.

449 The results obtained for the redundancy index, β_r , show that LA9, although less safe than LA3
450 and LA20 under a mainshock alone, is significantly more robust. These results can be correlated
451 to the LA9 building ability to distribute damage over its entire height of the building as shown in
452 Figure 9.

453 **CONCLUSIONS**

454 In this paper, a reliability-based robustness assessment methodology for steel moment resist-
455 ing frame structures subjected to post-mainshock seismic events was proposed and exemplified.
456 Robustness is computed through comparison of the structural reliability index under a mainshock,
457 considering the undamaged structure, and under an aftershock applied to the mainshock-damaged
458 structure. Probabilities of failure are computed through simulation, using nonlinear finite element
459 models that explicitly reproduce damage induced by strong shaking. The methodology is exempli-
460 fied using back-to-back mainshock-aftershock nonlinear dynamic time-history analyses.

461 For structures expected to form strong-column weak-beam failure mechanisms, a finite element
462 modeling approach was presented in which columns were modeled using force-based fiber-section
463 distributed plasticity elements and beams were modeled using a recently proposed phenomeno-
464 logical bilinear model with deterioration. The models used for the columns directly account for
465 axial load- bending moment interaction. For the beams, the deterioration behavior defined for the
466 plastic hinges is fundamental for accurate performance assessments under mainshock-aftershock
467 sequences. The finite-length plastic hinge element is used due to its ability to model plastic hinge
468 lengths explicitly and to separate the behavior of beam in the span from that of beam-column
469 connections.

470 Two-dimensional models of a 3-, 9-, and 20-story steel buildings, designed for the SAC project
471 for Los Angeles, California, were implemented in the OpenSees framework. For simulating the
472 mainshock-aftershock sequence of events, ten different mainshock and aftershock ground motion

473 records were combined. The spectral accelerations at fundamental periods of the buildings were
474 used to simulate mainshock and aftershock intensities that follow lognormal distributions. "Back-
475 to-back" mainshock-aftershock incremental dynamic analyses are performed for each combination
476 of mainshock-aftershock, while failure is defined in terms of the exceedance of an interstory drift
477 threshold. It is worth noting that the results presented here are sensitive to the frequency content of
478 the ground motions (both aftershock and mainshock), period elongation due to cyclic deterioration
479 in stiffness from the mainshock, and the definition of the fundamental period of the frame struc-
480 tures. These important factors are not considered herein, and as discussed in Faggella et al. (2013)
481 can only be adequately accounted for by using a vector-valued ground motion intensity measure.
482 The use of vector-valued ground motion intensity measures falls outside the scope of this paper.

483 Application of the reliability-based robustness assessment showed the importance of consid-
484 ering the aftershock in the evaluation of safety of structures under seismic events, as a significant
485 increase in failure probability was observed when mainshock-aftershock sequences were consid-
486 ered. Moreover, this study showed that the LA9 building, although initially more susceptible to
487 failure than the LA3 and LA20 buildings, presented significantly higher robustness for the af-
488 tershock events ($\beta_r = 41.52$ for LA9 versus $\beta_r = 19.32$ and $\beta_r = 11.31$ for LA3 and LA20,
489 respectively). In fact, robustness is defined in terms of the increase in probability of failure consid-
490 ering damage, and LA9, although less safe than LA3 and LA20 under a mainshock alone, presents
491 a lower reduction in reliability index when cascading events are considered. Thus, it can also be
492 concluded that the probabilities of failure for multiple hazards requires explicit modeling of the
493 hazards and simulation methods need to accurately model the damage induced by the cascading
494 hazards.

495 **ACKNOWLEDGEMENTS**

496 In the development of this research work, the first and third author would like to acknowl-
497 edge the support of the Portuguese Science and Technology Foundation through the fellowship
498 SFRH/BD/77722/2011 and UNIC Research Center at the New University of Lisbon. The support
499 of the School of Civil and Construction Engineering at Oregon State University to the second au-

500 thor is gratefully acknowledged. The first author would also like to acknowledge the support of
501 Oregon State University during the period in which he was a visiting Ph.D. student. The support
502 of the Nottingham Transportation Engineering Center to the third author is gratefully acknowl-
503 edged. The opinions and conclusions presented in this paper are those of the authors and do not
504 necessarily reflect the views of the sponsoring organizations.

505 **References**

506 Baker, J., Schubert, M., and Faber, M. (2008). "On the assessment of robustness." *Structural Safety*,
507 30(3), 253–267.

508 Baker, J. W. (2007). "Probabilistic structural response assessment using vector-valued intensity
509 measures." *Earthquake Engineering and Structural Dynamics*, 36(13).

510 Bommer, J. J. and Acevedo, A. B. (2004). "The use of real earthquake accelerograms as input to
511 dynamic analysis." *Journal of Earthquake Engineering*, 8(spec01), 43–91.

512 Cavaco, E., Casas, J., Neves, L., and Huespe, A. (2013). "Robustness of corroded reinforced con-
513 crete structures: a structural performance approach." *Structure and Infrastructure Engineering*,
514 9(1), 42–58.

515 Coleman, J. and Spacone, E. (2001). "Localization issues in force-based frame elements." *ASCE*
516 *Journal of Structural Engineering*, 127(11), 1257–1265.

517 Erduran, E. (2012). "Evaluation of rayleigh damping and its influence on engineering demand
518 parameter estimates." *Earthquake Engineering & Structural Dynamics*, 41(14), 1905–1919.

519 Faggella, M., Barbosa, A. R., Conte, J. P., Spacone, E., and Restrepo, J. I. (2013). "Probabilistic
520 seismic response analysis of a 3-d reinforced concrete building." *Structural Safety*, 44, 11–27.

521 FEMA355C (2000). *State of the Art Report on Systems Performance of Steel Moment Frames*
522 *Subjecte to Earthquake Ground Shaking*. SAC Joint Venture for the Federal Emergency Man-
523 agement Agency, Washington, DC.

524 FEMA356 (2000). "Prestandard and commentary for the seismic rehabilitation of buildings:
525 FEMA-356.

526 Fragiacomò, M., Amadio, C., and Macorini, L. (2004). "Seismic response of steel frames under
527 repeated earthquake." *Engineering Structures*, 26(13), 2021–2035.

528 Frangopol, D. and Curley, J. (1987). "Effects of damage and redundancy on structural reliability."
529 *ASCE Journal of Structural Engineering*, 113(7), 1533–1549.

530 Giberson, M. (1969). "Two nonlinear beams with definitions of ductility." *Journal of the Structural*
531 *Division*, 95(2), 137–157.

532 Gupta, A. and Krawinkler, H. (1999). "Seismic demands for performance evaluation of steel mo-
533 ment resisting frame structures." *Report No. 132*, The John A. Blume Earthquake Engineering
534 Center.

535 Haselton, C. and Deierlein, G. (2007). "Assessomg seismic collapse safety of modern reinforced
536 concrete frame buildings." *Report No. 156*, The John A. Blume Earthquake Engineering Center,
537 Stanford University.

538 Ibarra, L. F. and Krawinkler, H. (2005). "Global collapse of frame structures under seismic exci-
539 tations." *Report No. 152*, The John A. Blume Earthquake Engineering Research Center, Depart-
540 ment of Civil Engineering, Stanford University, Stanford, CA.

541 Jayaram, N. and Baker, J. (2008). "Statistical tests of the joint distribution of spectral acceleration
542 values." *Bulletin of the Seismological Society of America* 2008, 98(5), 2231–2243.

543 Kiureghian, A. D. (1996). "Structural reliability methods for seismic safety assessment: a review."
544 *Engineering Structures*, 18(6), 412 – 424.

545 Lee, K. and Foutch, D. (2004). "Performance evaluation of damaged steel frame buildings sub-
546 jected to seismic loads." *ASCE Journal of Structural Engineering*, 130(4), 588–599.

547 Li, Q. and Ellingwood, B. R. (2007). "Performance evaluation and damage assessment of steel
548 frame buildings under main shock-aftershock earthquake sequences." *Earthquake Engineering*
549 *& Structural Dynamics*, 36(3), 405–427.

550 Li, Y., Song, R., van de Lindt, J., Nazari, N., and Luco, N. (2012). "Assessment of wood and steel
551 structures subjected to earthquake mainshock-aftershock." *XV World Conference on Earthquake*
552 *Engineering*, Lisbon, Portugak.

553 Lignos, D. and Krawinkler, H. (2012). "Development and utilization of structural component
554 databases for performance-based earthquake engineering." *ASCE Journal of Structural Engi-*
555 *neering*.

556 Lignos, D. G., Chung, Y., Nagae, T., and Nakashima, M. (2011). "Numerical and experimen-
557 tal evaluation of seismic capacity of high-rise steel buildings subjected to long duration earth-
558 quakes." *Comput. Struct.*, 89(11-12), 959–967.

559 Lignos, D. G. and Krawinkler, H. (2011). "Deterioration modeling of steel components in sup-
560 port of collapse prediction of steel moment frames under earthquake loading." *ASCE Journal of*
561 *Structural Engineering*, 137(11), 1291–1302.

562 Lind, N. C. (1995). "A measure of vulnerability and damage tolerance." *Reliability Engineering*
563 *and System Safety*, 48(1), 1–6.

564 Luco, N. (2002). "Probabilistic seismic demand analysis, SMRF connection fractures, and near-
565 source effects." Ph.D. thesis, Department of Civil and Environmental Engineering, Stanford
566 University, Stanford, California.

567 Luco, N., Bazzurro, P., and Cornell, C. (2004). "Dynamic versus static computation of the residual
568 capacity of a mainshock-damaged building to withstand an aftershock." *13th World Conference*
569 *on Earthquake Engineering*, Vancouver, Canada.

570 Luco, N. and Cornell, C. A. (2000). "Effects of connection fractures on smrf seismic drift de-
571 mands." *ASCE Journal of Structural Engineering*, 126(1), 127–136.

572 Luco, N., Gerstenberger, M. C., Uma, S., Ryu, H., Liel, A. B., and Raghunandan, M. (2011).
573 "A methodology for post-mainshock probabilistic assessment of building collapse risk." *Pacific*
574 *Conference on Earthquake Engineering*, Auckland, New Zealand (April).

575 Mazzoni, S., McKenna, F., Scott, M. H., and Fenves, G. L. (2009). *The OpenSees command lan-*
576 *guage manual, Version 2.0*. Pacific Earthquake Eng. Research Center, Univ. California at Berke-
577 ley.

578 Medina, R. and Krawinkler, H. (2005). "Evaluation of drift demands for the seismic performance
579 assessment of frames." *ASCE Journal of Structural Engineering*, 131(7), 1003–1013.

580 Newell, J. D. and Uang, C.-M. (2008). "Cyclic behavior of steel wide-flange columns subjected to
581 large drift." *Journal of structural engineering*, 134(8), 1334–1342.

582 Newmark, N. and Rosenbleuth, E. (1971). *Fundamental of Earthquake Engineering*. Prentice-Hall.

583 PEER/ATC (2010). "Modeling and acceptance criteria for seismic design and analysis of tall build-
584 ings." *Report No. 72-1*, ATC - Applied Techonology Council.

585 Petersen, M., Frankel, A., Harmsen, S., Mueller, C., Haller, K., Wheeler, R., Wesson, R., Zeng,
586 Y., Boyd, O., Perkins, D., Luco, N., Field, E.H. Wills, C., and Rukstales, K. (2008). "Documen-
587 tation for the 2008 update of the united states national seismic hazard maps." *Report no.*, U.S.
588 Geological Survey Open-File Report 2008-1128. 61 p.

589 Prakash, V., Powell, G., and Campbell, S. (1993). "Drain-2dx base program description and user
590 guide, version 1.0." *Report No. UCB/SEMM-93/17-18*, Engineering Mechanics and Material,
591 Department of Civil Engineering, University of California, Berkeley, CA.

592 Ribeiro, F., Barbosa, A., and Neves, L. (2012). "Numerical analysis of steel moment resisting
593 frames under mainshock-aftershock seismic sequences." *Report No. Kiewit - 2012/07*, Oregon
594 State University.

595 Ruiz-García, J. (2012). "Mainshock-aftershock ground motion features and their influence in build-
596 ing's seismic response." *Journal of Earthquake Engineering*, 16(5), 719–737.

597 Ryu, H., Luco, N., Uma, S., and Liel, A. (2011). "Developing fragilities for mainshock-damaged
598 structures through incremental dynamic analysis." *Pacific Conference on Earthquake Engineer-*
599 *ing*, Auckland, New Zealand (April).

600 Scott, M. and Ryan, K. (2013). "Moment-rotation behavior of force-based plastic hinge elements."
601 *Earthquake Spectra*, 29(1).

602 Scott, M. H. and Fenves, G. L. (2006). "Plastic hinge integration methods for force-based beam-
603 column elements." *ASCE Journal of Structural Engineering*, 132(2), 244–252.

604 Somerville, P., Smith, N., Punyamurthula, S., and Sun, J. (1997). "Development of ground mo-
605 tion time histories for phase ii of the fema/sac steel project." *Report No. SAC/BD-97/04*, SAC
606 Background Document.

607 Starossek, U. (2006). "Progressive collapse of structures: Nomenclature and procedures." *Struc-*
608 *tural Engineering International*, 2(16), 113–117.

609 Starossek, U. and Haberland, M. (2008). "Measures of structural robustness—requirements and
610 applications." *ASCE SEI Structures Congress - Crossing Borders*, Vancouver, Canada.

611 Thain, D., Tannenbaum, T., and Livny, M. (2005). "Distributed computing in practice: the condor
612 experience.." *Concurrency - Practice and Experience*, 17(2-4), 323–356.

613 UBC (1994). "*Structural Engineering Design Provisions*", *Uniform Building Code, Vol. 2*. Inter-
614 national Conference of Building Officials.

615 Vamvatsikos, D. and Cornell, C. (2002). "Incremental dynamic analysis." *Earthquake Engineering*
616 *and Structural Dynamics*, 31(3), 491–514.

617 Yeo, G. L. and Cornell, C. (2005). "Stochastic characterization and decision bases under time-
618 dependent aftershock risk in performance-based earthquake engineering." *Report no.*, Pacific
619 Earthquake Engineering Research Center - College of Engineering. PEER Report 2005/13.

List of Tables

621	1	Models description	26
622	2	Periods of vibration for OpenSees models and FEMA355C model	27
623	3	Mean relative difference in peak interstory drift ratio to model M1 (FEMA355C	
624		2000)	28
625	4	Probabilities of failure, reliability indexes and redundancy index associated with	
626		the scenarios considered	29

Table 1. Models description

Model	Columns		Beams	
	Element formulation	Material	Element formulation	Material
FZLH	Force-based fiber-section distributed plasticity	Elasto-plastic with hardening	Zero-length (Concentrated plasticity)	Elasto-plastic with Hardening
FZLB				Bilinear with deterioration (<i>Bilin</i>)
FMRH			Finite-length plastic hinge (Modified-Radau)	Elasto-plastic with Hardening
FMRB				Bilinear with deterioration (<i>Bilin</i>)

Table 2. Periods of vibration for OpenSees models and FEMA355C model

	LA3 Building		LA9 Building		LA20 Building	
	OpenSees	FEMA355C	OpenSees	FEMA355C	OpenSees	FEMA355C
1 st Mode	1.04s	1.03s	2.40s	2.34s	4.10s	3.98s
2 nd Mode	0.34s	0.33s	0.90s	0.88s	1.40s	1.36s
3 rd Mode	0.18s	0.17s	0.52s	0.50s	0.81s	0.79s

Table 3. Mean relative difference in peak interstory drift ratio to model M1 (FEMA355C 2000)

Building	Model			
	FZLH	FMRH	FMRB	FZLB
LA3	4.6%	4.0%	5.6%	8.7%
LA9	4.5%	5.1%	6.4%	8.4%
LA20	7.4%	6.3%	9.3%	9.8%

Table 4. Probabilities of failure, reliability indexes and redundancy index associated with the scenarios considered

Scenario		LA3 Building	LA9 Building	LA20 Building
Mainshock	Probability of failure (p_{f1})	3.56×10^{-4}	7.22×10^{-4}	6.17×10^{-4}
	Reliability index (β)	3.38	3.19	3.23
Mainshock \cup Aftershock	Probability of failure (p_{f3})	1.02×10^{-3}	1.66×10^{-3}	2.23×10^{-3}
	Reliability index (β)	3.08	2.94	2.84
Aftershock Mainshock	Probability of failure (p_{f2})	6.64×10^{-4}	9.39×10^{-4}	1.61×10^{-3}
	Reliability index (β)	3.21	3.11	2.95
Redundancy index β_r		19.32	41.52	11.31

List of Figures

628	1	Flowchart for the robustness assessment of buildings subjected to cascading seismic events	32
629			
630	2	Building Models (a) LA3; (b) LA9; (c) LA20; and (d) P-M interaction curve	33
631	3	Adapted modified Ibarra-Krawinkler model: (a) backbone curve; and (b) basic modes of cyclic deterioration	34
632			
633	4	LA3 building - Nonlinear static (pushover) capacity curve considering a 1 st mode lateral load pattern	35
634			
635	5	LA9 building - Nonlinear static (pushover) capacity curve considering a 1 st mode lateral load pattern	36
636			
637	6	LA20 building - Nonlinear static (pushover) capacity curve considering a 1 st mode lateral load pattern	37
638			
639	7	LA3 building - Example of a mainshock-aftershock back-to-back acceleration and drift response time-histories	38
640			
641	8	LA3 building hinge moment-rotation response at: (a) bottom of first story in grid line A; (b) left end of first floor level beam A-B	39
642			
643	9	Deformed shapes of the buildings at two different instants: (a,c,d) - Peak interstory drift ratio during the mainshock; and (b,d,f) - Peak interstory drift ratio during the aftershock, for LA3, LA9 and LA20, respectively.	40
644			
645			
646	10	LA3 building - Aftershock IDA curves for ten earthquake records and four different mainshock ground motion spectral accelerations	41
647			
648	11	LA3 building - Aftershock ground motion spectral acceleration at the fundamental period of the intact structure that leads to failure as a function of the mainshock ground motion spectral acceleration for earthquake E5	42
649			
650			

651 12 Median lowest aftershock ground motion spectral acceleration at the fundamen-
652 tal period of the intact structure that leads to failure (solid line and left vertical
653 axis) and median residual interstory drift ratio after mainshock (dashed line and
654 right vertical axis) as a function of the median mainshock ground motion spectral
655 acceleration 43

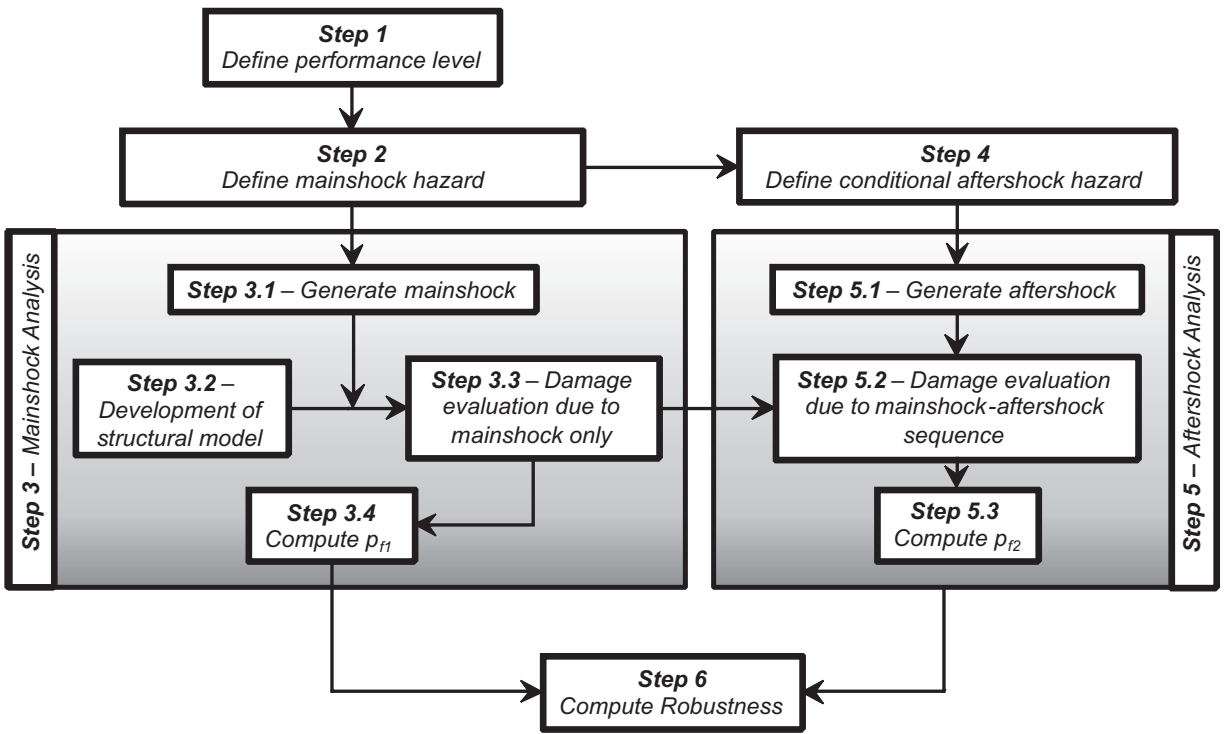


Figure 1. Flowchart for the robustness assessment of buildings subjected to cascading seismic events

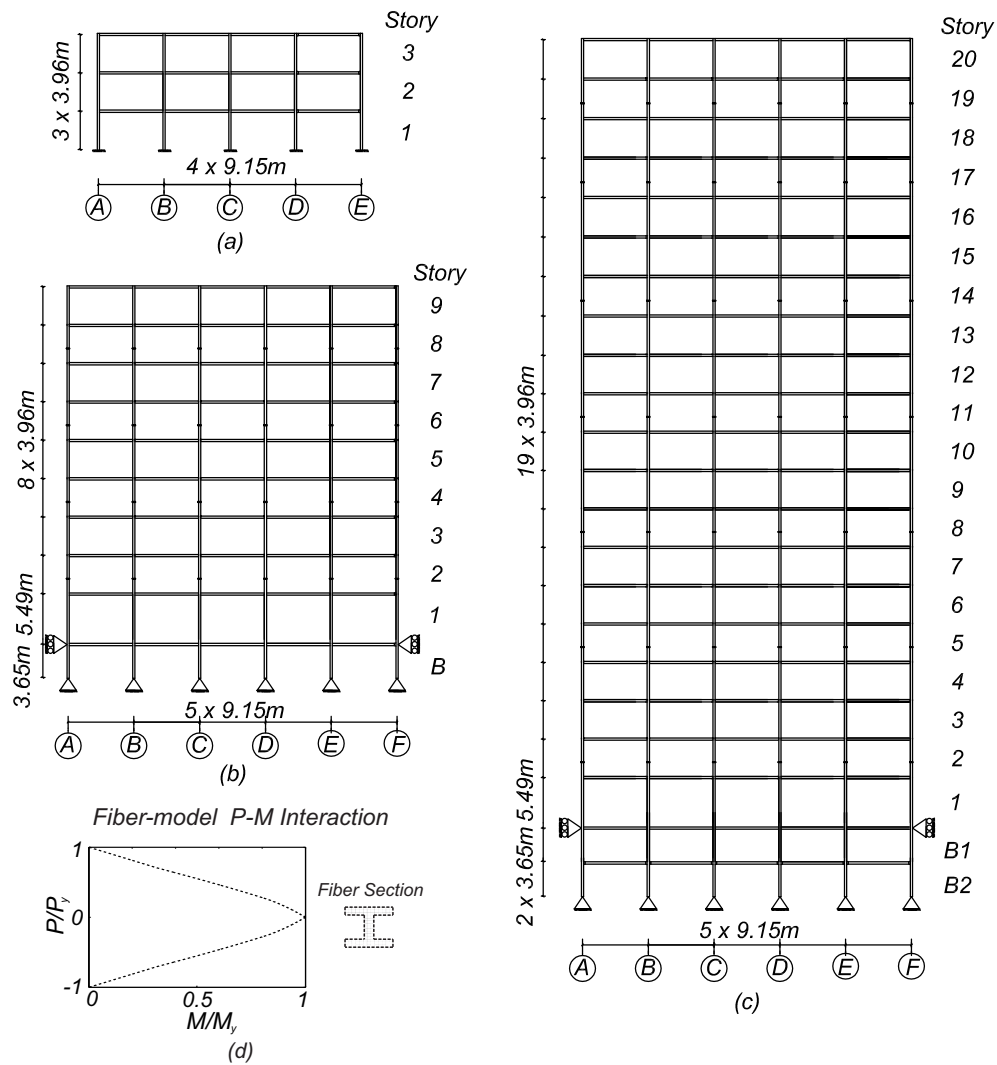


Figure 2. Building Models (a) LA3; (b) LA9; (c) LA20; and (d) P-M interaction curve

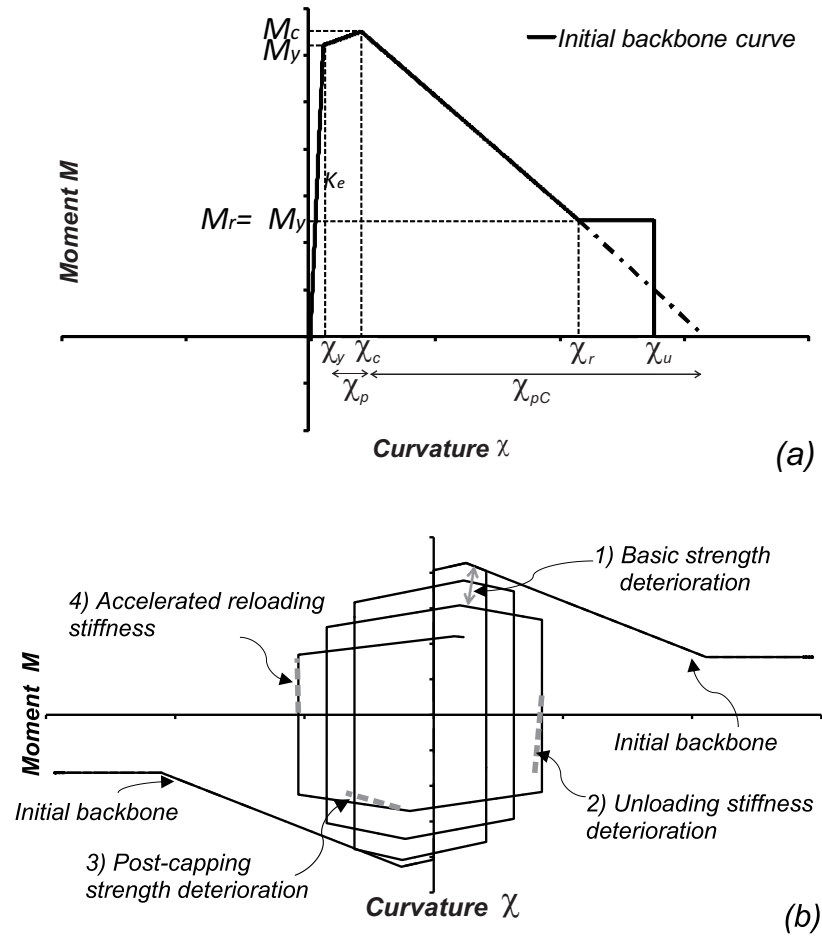


Figure 3. Adapted modified Ibarra-Krawinkler model: (a) backbone curve; and (b) basic modes of cyclic deterioration

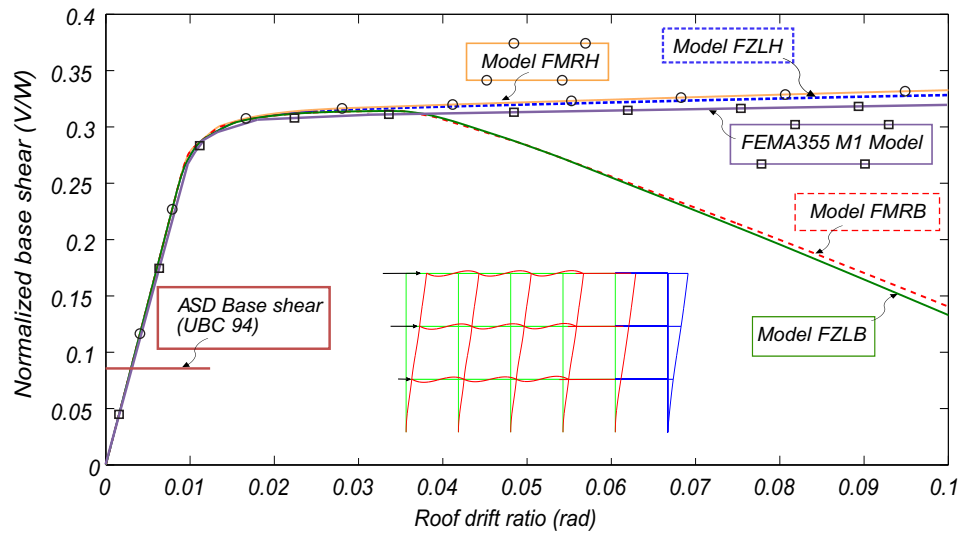


Figure 4. LA3 building - Nonlinear static (pushover) capacity curve considering a 1st mode lateral load pattern

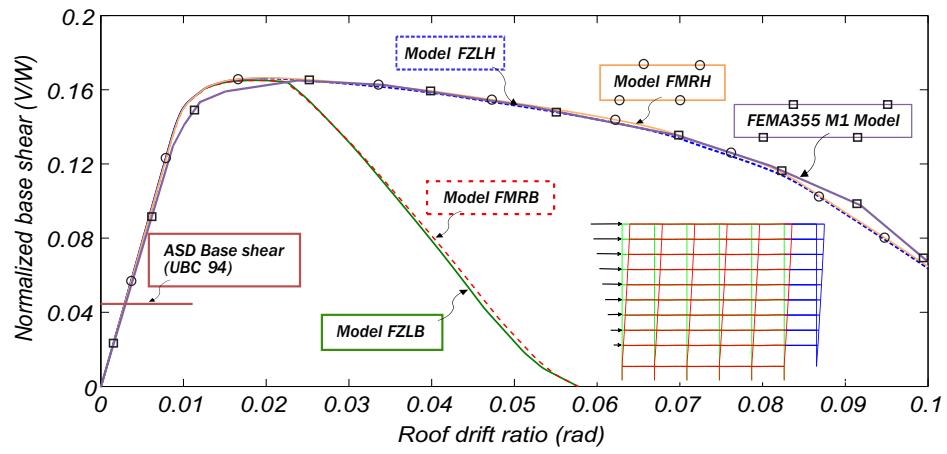


Figure 5. LA9 building - Nonlinear static (pushover) capacity curve considering a 1st mode lateral load pattern

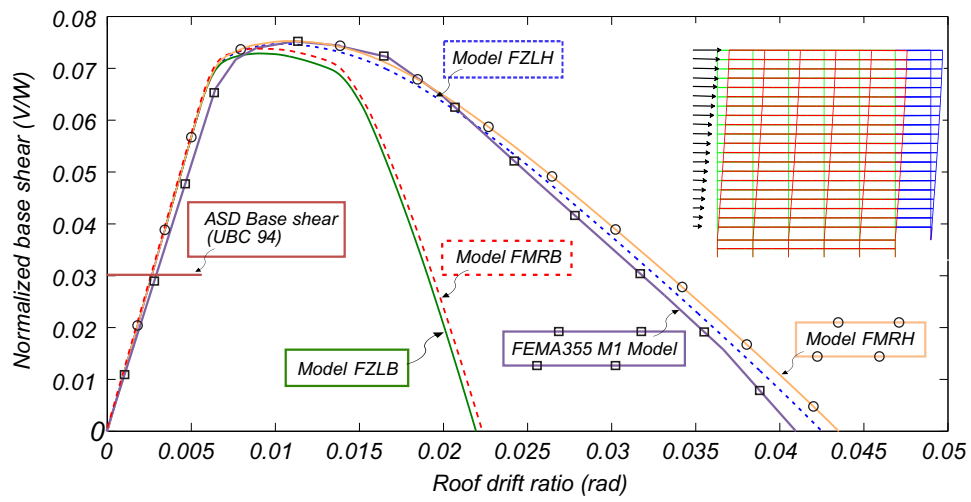


Figure 6. LA20 building - Nonlinear static (pushover) capacity curve considering a 1st mode lateral load pattern

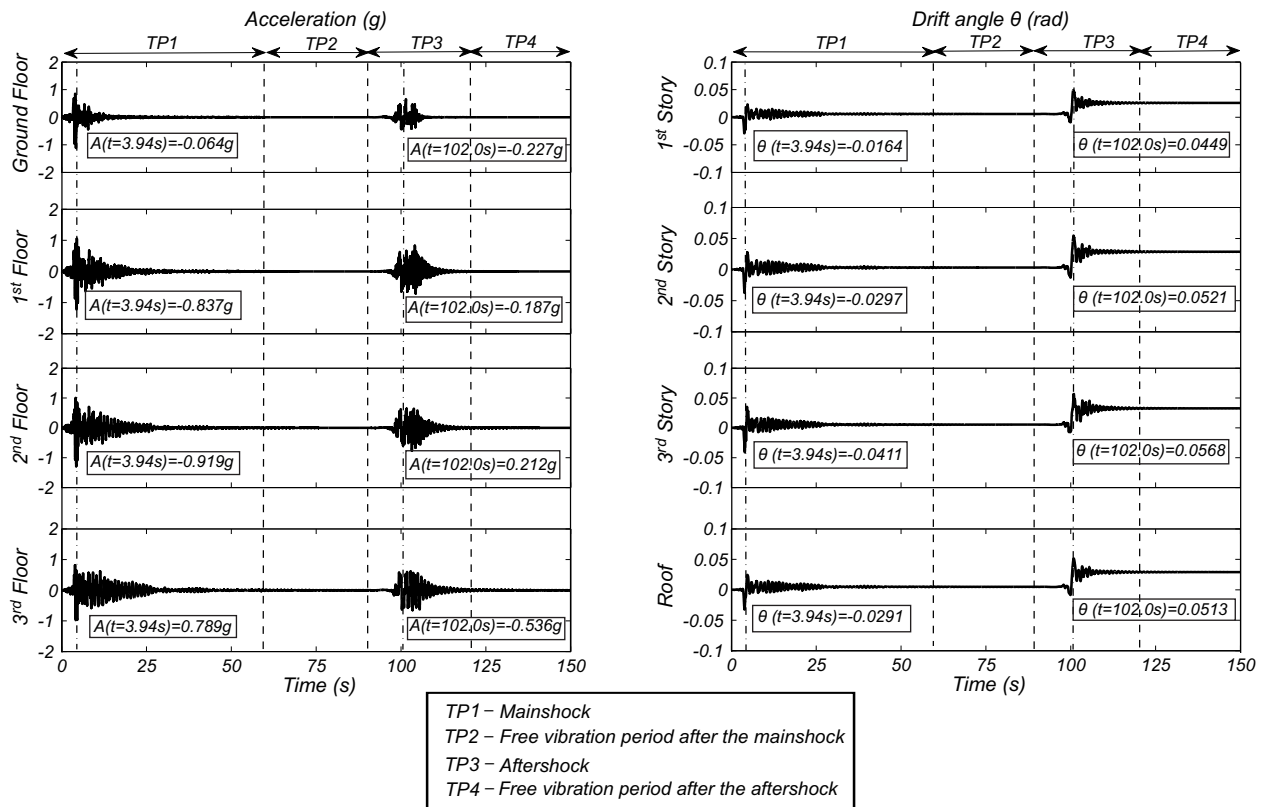


Figure 7. LA3 building - Example of a mainshock-aftershock back-to-back acceleration and drift response time-histories

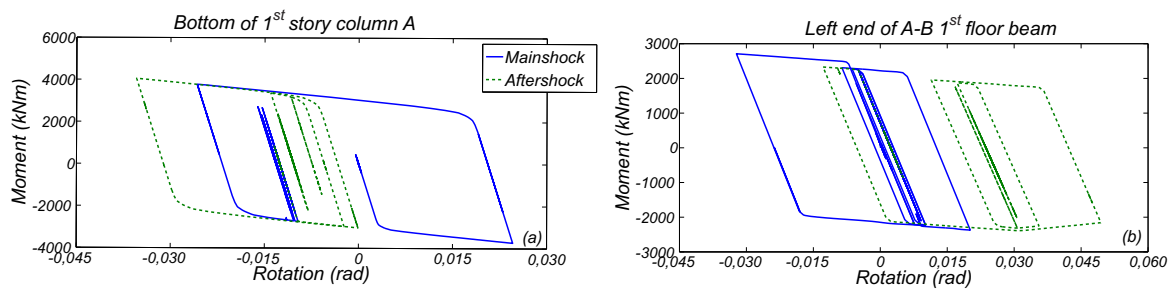


Figure 8. LA3 building hinge moment-rotation response at: (a) bottom of first story in grid line A; (b) left end of first floor level beam A-B

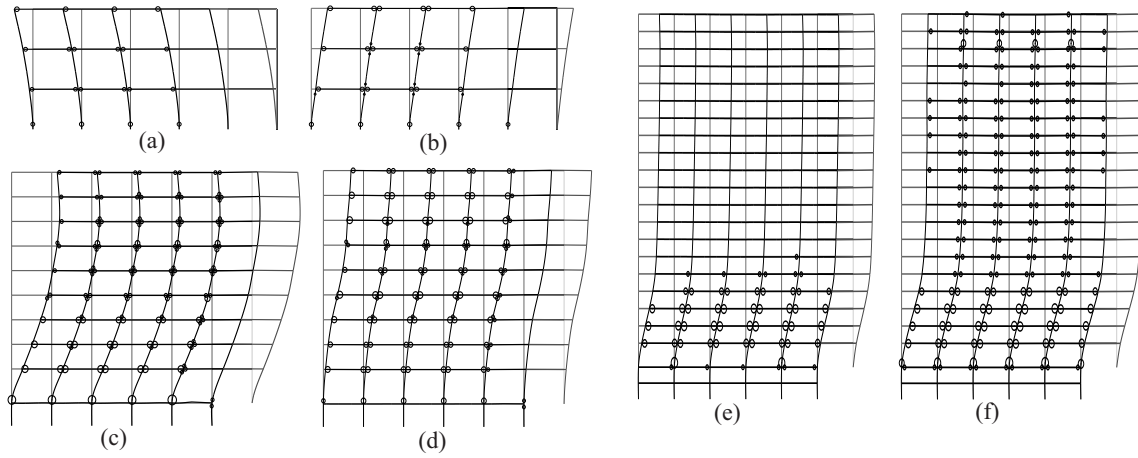


Figure 9. Deformed shapes of the buildings at two different instants: (a,c,d) - Peak interstory drift ratio during the mainshock; and (b,d,f) - Peak interstory drift ratio during the aftershock, for LA3, LA9 and LA20, respectively.

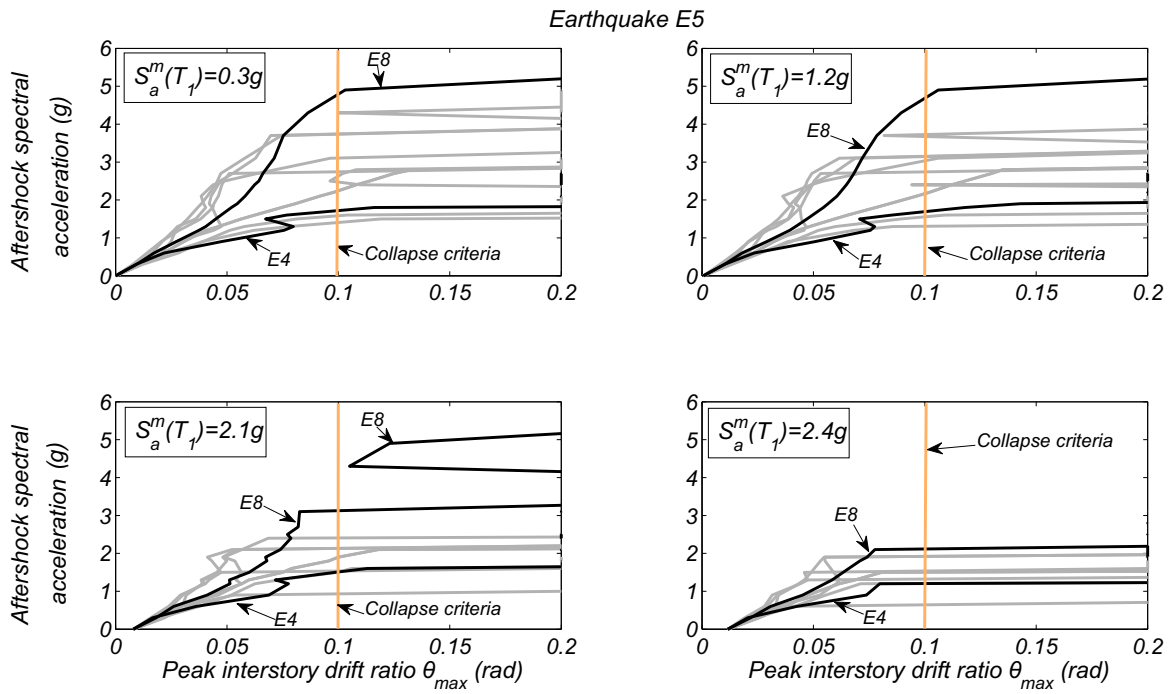


Figure 10. LA3 building - Aftershock IDA curves for ten earthquake records and four different mainshock ground motion spectral accelerations

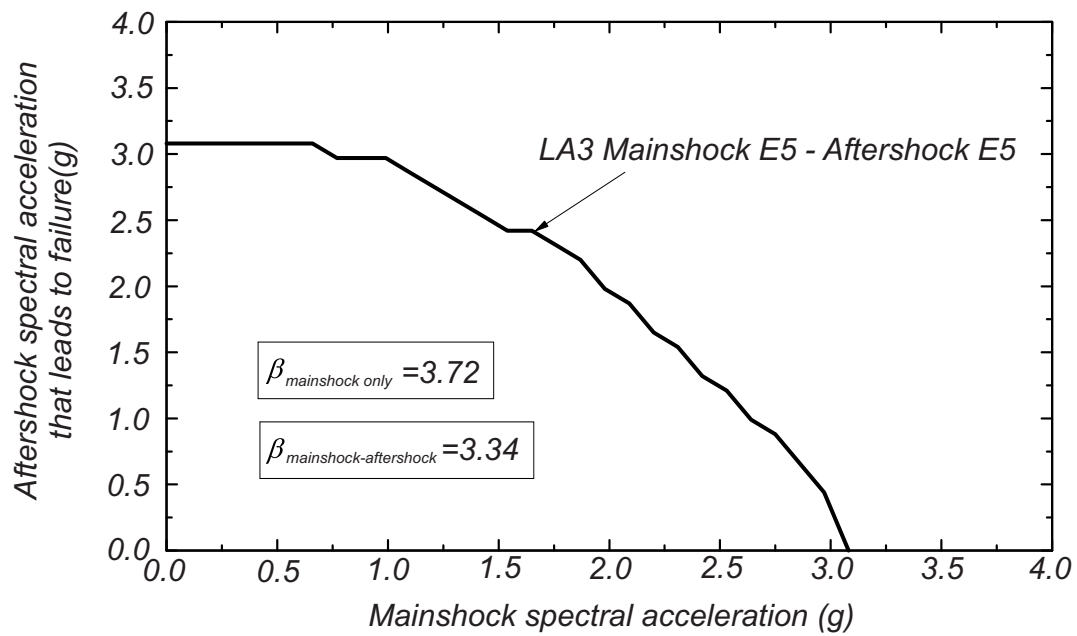


Figure 11. LA3 building - Aftershock ground motion spectral acceleration at the fundamental period of the intact structure that leads to failure as a function of the mainshock ground motion spectral acceleration for earthquake E5

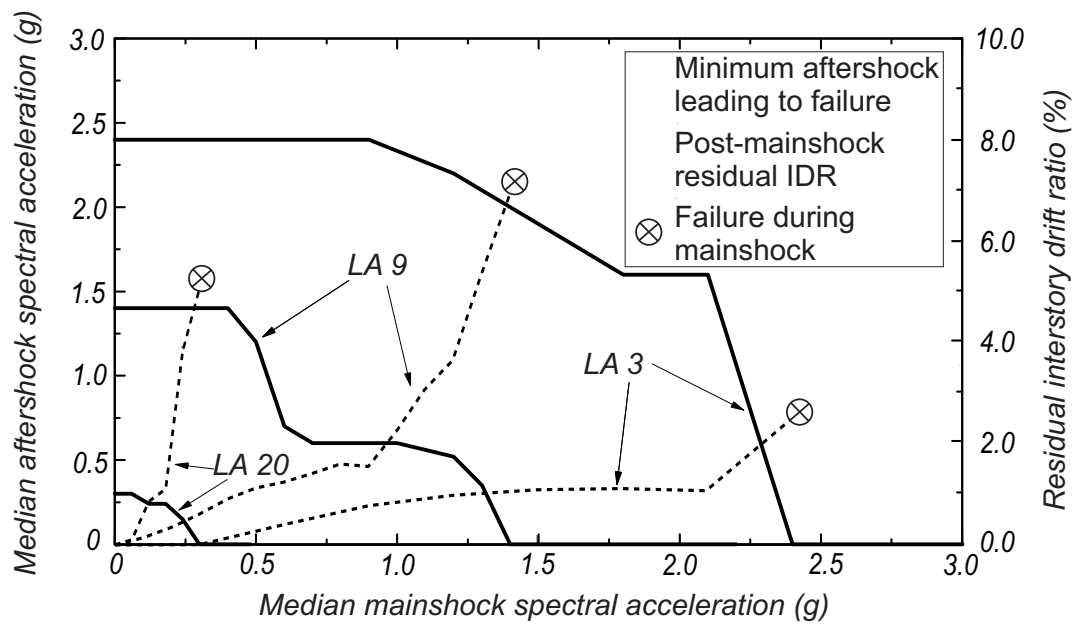


Figure 12. Median lowest aftershock ground motion spectral acceleration at the fundamental period of the intact structure that leads to failure (solid line and left vertical axis) and median residual interstory drift ratio after mainshock (dashed line and right vertical axis) as a function of the median mainshock ground motion spectral acceleration